

Optical, Physical, Chemical and Electrical Properties of Nickel Oxide Sprayed Thin Films under Tin Doping Effects

M. Ben Amor^a, N. Hamzaoui^b, A. Boukhachem^a, C. Mrabet^a, M. Ghamnia^b, A. Yumak^c, K. Boubaker^{a,*}, P. Petkova^d, M. Amlouk^a

^a Unité de Physique des dispositifs à Semi-conducteurs UPDS, Faculté des Sciences de Tunis, Campus Universitaire, 2092 Tunis, TUNISIE.

^b Laboratoire LSMC, Université d'Oran 1, 31000, Oran, ALGERIE.

^c Physics Department, Faculty of Arts and Sciences, Marmara University, 34722 Göztepe, Istanbul, TURKEY

^d Faculty of Natural Sciences, Shumen University "Konstantin Preslavsky", 115 Universitetska street, Shumen, BULGARIA

ipwbp@yahoo.fr *

Abstract

Tin-doped nickel oxide thin films have been successfully prepared by spray pyrolysis technique on glass substrates at 460°C. The effects of tin doping on structural, optical, and electrical properties were investigated. X-ray diffraction pattern reveals that all prepared thin films have cubic structure with (111) preferred orientation. The surface topography of these films was performed by atomic force microscopy. Optical measurements show a high transparency in the visible range around 95%. The optical band gap E_g decreases with Sn content from 3.633 to 3.54 eV. PL measurements show some bands transition which shift irregularly with Sn doping. Finally, the electric conductivity of NiO thin film was investigated through the impedance spectroscopy measurements in the frequency range 5 Hz-13 MHz at various temperatures. These measurements show a thermally activation of the electric. AC conductivity of NiO thin films is investigated through Jonscher law. Also, from these measurements, dielectric parameters were calculated.

Keywords

Nickel Oxide; Doping; Thin Films; Raman Modes; Microstructure; Optical Properties

Introduction

Transparent conducting oxides (TCOs) such as zinc oxide [1], tin oxides [2] and indium oxide [3] have been attracted much attentions due to of their chemical and thermal stability.

Among these oxides, nickel oxide (NiO) has attracted considerable attention from those interested in the application to devices working in ultraviolet regions, with the interest specially lying in its wide band gap [4].

It has been recorded that NiO is a cubic structured [5] with anti-ferromagnetic and electro-chromic properties [6-10]. This material has important properties which are explored for several applications such as smart windows [11], dye sensitized photocathode [12], transparent p-type semi-conductors [13, 14], and gas sensors [15- 17].

NiO thin films have been prepared by various methods such as sputtering [18, 19], sol gel [20], pulsed laser deposition [21, 22], chemical vapor deposition [23, 24], and spray pyrolysis [25, 26]. Among these techniques, spray pyrolysis is the widely used; it is an attractive process to obtain thin films which requires low cost raw materials, adherent of deposits, very easy, safe and cheap. Furthermore, this technique leads to a large production area and it is special to give crystallized thin films without recourse to thermal processing

Its deposition on glass like substrates has been widely experimented and applied [27- 29]. On the other hand, NiO has been the subject of many research works in terms of doping. Several elements were used as a doping to improve some physical properties such as Mg [27], Cu [30, 31], In [32], Li [33] and K [34].

The present work aims to reach the synthesis of NiO: Sn thin films using the spray pyrolysis technique. These films

have been investigated by using XRD, optical reflectance and transmission spectra, PL measurements. On the other hand, an attempt regarding their electrical properties has been carried out by means of the conductivity measurements in terms of both temperature and frequency.

Experimental Details

Thin Films Preparation and Characterization Techniques

Tin-doped NiO thin films were synthesized by spray pyrolysis method on glass substrates at 460° C. Aqueous starting solutions containing the desired composition of corresponding cations were prepared by dissolving Nickel(II) chloride hexahydrate ($\text{NiCl}_2 \cdot 6\text{H}_2\text{O}$) 10^{-2} M (ACROS Organic pure more than 99 %), and Tin(II) chloride dehydrate ($\text{SnCl}_2 \cdot 2\text{H}_2\text{O}$) (ACROS Organics pure more than 98%). The molar ratio $x = [\text{Sn}] / [\text{Ni}]$ varies from 0% to 4%. Acetic acid was added to ensure good solubility and a better homogeneity of the starting solution. Nitrogen was used as the carrier gas (pressure at 0.35 bar) through a 0.5 mm-diameter nozzle. As reported previously [35], the nozzle-to-substrate plane distance was fixed at the optimal value of 27 cm. During the deposition process, the precursor mixture flow rate was taken constantly at 4 mL/min. finally; spraying temperature was fixed at 450°C. This temperature seems optimal for this II-VI binary thin films preparation [27, 28].

The X-ray diffraction analysis of all prepared thin films was performed by a copper-source diffractometer (Analytical X-Pert PROMPD), with the wavelength ($\lambda = 1.5406 \text{ \AA}$). Morphological aspects and surface topography of the films were examined by atomic force microscopy (AFM) (Park Scientific Instrument) in contact mode. The optical measurements, in the UV-visible range were carried out using a Shimadzu UV 3100 double-beam spectrophotometer, within a (250–2500 nm) wavelength range.

Finally, the configuration for electrical measurements was performed using two-electrodes which were applied onto the two extremities of the sample using silver paste (figure 1).

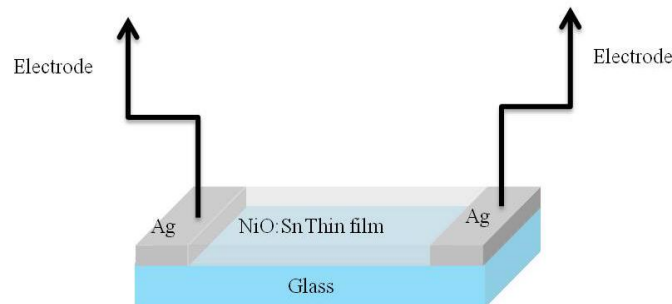


FIG.1: CONFIGURATION FOR ELECTRICAL MEASUREMENTS

Real and imaginary components of impedance parameters (Z' and Z'') were made over a wide range of temperature 300-420°C and frequency 5 Hz - 13 MHz by means of a Hewlett-Packard HP 4192 impedance analyzer at 120 frequencies, log-scaled between 5 Hz and 13 MHz by applying a sinusoidal signal of 50 mV whose principle set up is displayed in Figure 2.

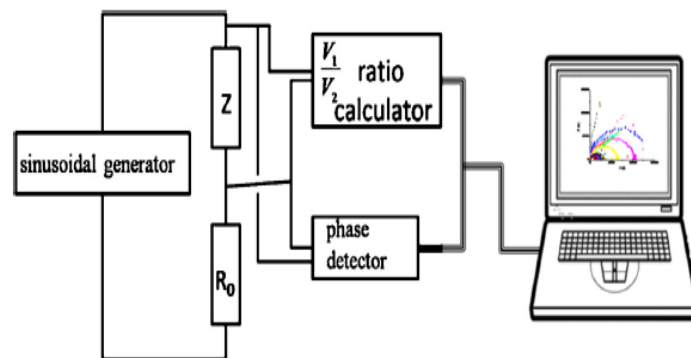


FIG.2: SCHEMATIC PRINCIPLE OF MOUNTING IMPEDANCE MEASUREMENT

Results and Discussion

Structural Analyses

Figure 3 shows the XRD patterns of tin-doped nickel oxide sprayed thin films. From the XRD patterns, it is found that all samples exhibit cubic phase according to JCPDS: 04-0835 card with (111) preferential orientation. This indicates that the structures of doped NiO are not altered by the incorporation of Sn doping. It is also worth noting that no peak related to tin oxide has been found in these spectra. This is probably due to the low Sn content (< 5%), which indicates that tin ions substitute positions and have not changed the cubic structure of NiO.

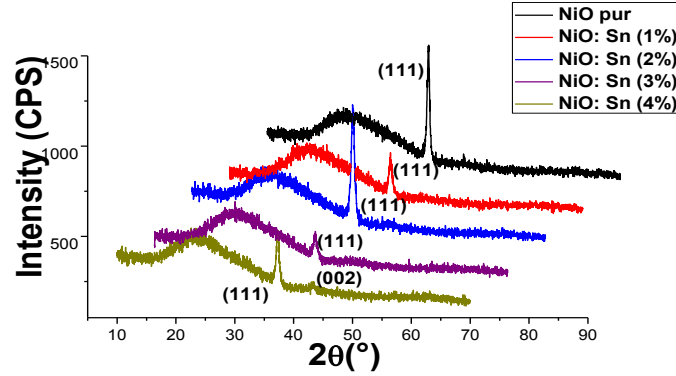


FIGURE 3: XRD PATTERNS OF UNDOPED NIO AND DOPED SN THIN FILMS.

The interplanar spacing of given Miller indices h , k and l d_{hkl} values of NiO: Sn thin films were also calculated by using Bragg equation:

$$2d_{hkl} \sin \theta = n\lambda \quad (1)$$

Where n is the order of diffraction (usually $n = 1$) and λ is the X-ray wavelength. Table 1 summarizes the calculated values of d_{111} of the prepared NiO: Sn thin films.

In the NiO cubic structure, the plane spacing is related to the lattices parameters a and Miller indexes by the following relation [27]:

$$d_{hkl} = \frac{a}{\sqrt{h^2 + k^2 + l^2}} \quad (2)$$

The calculated value of lattice parameter is listed in table 1. It is found that this parameter decreases with Sn content from 4.1742 Å to 4.1666 Å.

TABLE 1: CALCULATED VALUE OF LATTICE PARAMETER

	$2\theta (^{\circ})$	$d_{111}(\text{\AA})$	$a (\text{\AA})$
NiO pur	37.3798	2,4038	4.1635
NiO: Sn 1 %	37.2805	2,4100	4.1742
NiO: Sn 2 %	37.4026	2,4024	4.1611
NiO: Sn 3 %	37.3300	2,4069	4.1689
NiO: Sn 4 %	37.3821	2,4056	4.1666

The high value is obtained at 1% Sn doping level. This particular $[\text{Sn}]/[\text{Ni}]$ ration seems an appropriate value for possibly incorporation inside the nickel oxide thin film. Indeed, the compactness of the host material increases which suggests that Sn doping can play an important role in improving some physical properties of such II-VI binary thin films.

This change in the lattice parameter with the doping level may change more physical properties of this oxide and thereafter may give the appropriate doping levels for potential applications using nickel oxide.

XRD spectra were also used to study the effect of incorporation of the element Sn in the NiO matrix respectively on the crystallite size, using the formula Debye-Scherrer [36, 37], the stress [38] and dislocation density [39, 40]

$$\left\{ \begin{array}{l} D = \frac{k \cdot \lambda}{\beta_{\frac{1}{2}} \cos(\theta)} \\ \xi = \frac{\beta_{\frac{1}{2}}}{4 \tan(\theta)} \\ \delta = \frac{1}{D^2} \end{array} \right. \quad (3)$$

$$\xi = \frac{\beta_{\frac{1}{2}}}{4 \tan(\theta)} \quad (4)$$

$$\delta = \frac{1}{D^2} \quad (5)$$

Where $k = 0.90$ is the Scherrer constant, $\beta_{1/2}$ is the corrected half width of the peak and $\lambda = 1.5406 \text{ \AA}$ is the wavelength of $\text{CuK}\alpha$ radiation.

The calculated values of these parameters are gathered in table 2.

TABLE 2: VALUES OF GRAINS SIZE, MICRO-STRAIN AND DISLOCATION DENSITY

	D (nm)	ϵ (10^{-4})	δ ($10^{13} \text{ Lines/m}^2$)
NiO	293,88	36,84	1,16
NiO: Sn 1 %	128,53	84,44	6,05
NiO: Sn 2 %	228,58	47,33	1,91
NiO: Sn 3 %	205,68	52,70	2,36
NiO: Sn 4 %	228,07	47,46	1,92

From the calculated values of these structural parameters, it can be seen the particularity of 1% Sn doping level is consistent with the effect on the lattice parameter described above.

Morphological Characterization

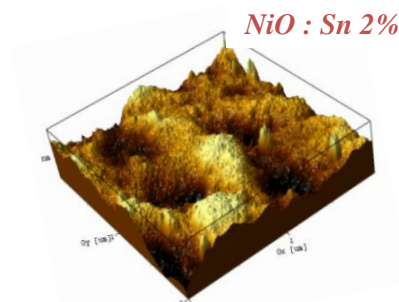
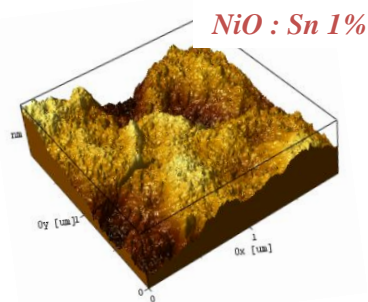
Figure 4 shows 3D topography performed with Atomic Force Microscope of tin doped NiO thin films. The root mean square roughness (R_q) values were obtained from AFM observations and calculated using the following relation [41]:

$$R_q = \sqrt{\frac{1}{N} \sum (Z_m - Z_t)^2} \quad (6)$$

R_q values are listed in table 3.

TABLE 3: VALUES OF RMS ROUGHNESS OF SN DOPED NIO THIN FILMS

	RMS Roughness (nm)
Pure NiO	16.6 [27]
NiO: Sn 1%	14.38
NiO: Sn 2%	16.3
NiO: Sn 3%	9.5
NiO: Sn 4%	27.9



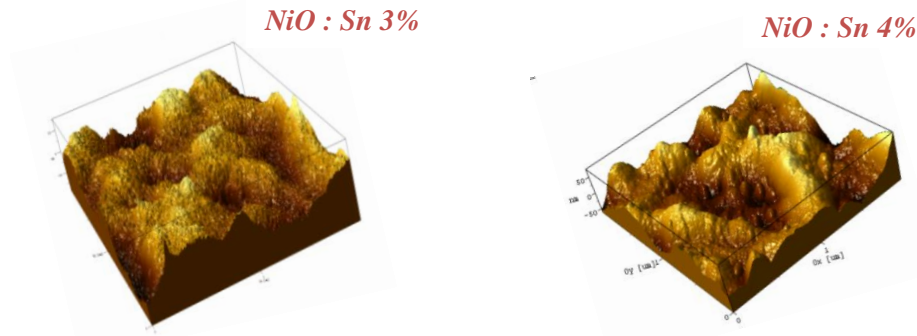


FIGURE 4: UNDOPED AND DOPED NIO: SN LAYERS AFM 3D SURFACE TOPOGRAPHY

In comparison with crystallite size, roughness values show a very smooth surface of the sample. In the same line, these values are less than the thickness of prepared films; this property seems good for optical applications.

Optical Properties

1) Band Gap Energy Calculation

Spectral transmittance $T(\lambda)$ and reflectance $R(\lambda)$ were measured in the wavelength range of 300 - 2500 nm using UV-Visible SHIMADZU double beam spectrophotometer. Figure 5 shows transmittance and reflectance spectra vs. wavelength of NiO: Sn thin films at different Sn contents.

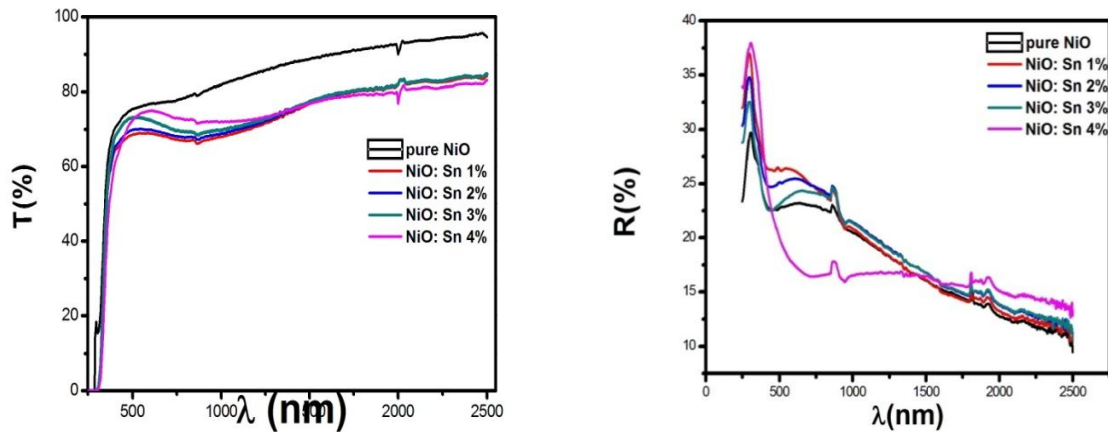


FIGURE 5: TRANSMITTANCE AND REFLECTANCE SPECTRA OF NIO: SN THIN FILMS

The spectra show a high transmittance of all prepared thin films (higher than 80%) and low reflectance. This property offers the possibility of using this material as an optical window.

Also, it is found that the transmittance increases and reflectance decreases with tin doping. This doping type can encourage the use of this oxide as an optical window.

The optical band gap calculated from the transmission measurements is given by [42]:

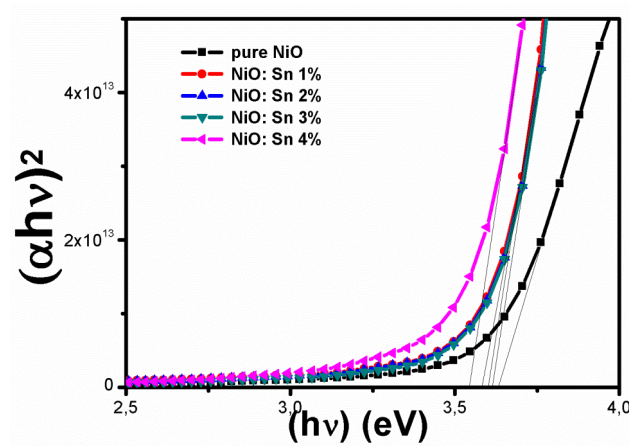
$$\alpha(\lambda) = \frac{1}{d} \ln \frac{1}{T(\lambda)} \quad (7)$$

As NiO is a direct semiconductor transition, optical band gap can be deduced by using the following relation [43-45]

$$(\alpha h\nu)^2 = A(h\nu - E_g) \quad (8)$$

Where: A is a constant, $h\nu$ is the photon energy, E_g is the optical band gap energy E_g

Optical band gap width values were extracted from absorption edge every sample from the intercept of $(\alpha h\nu)^2$ versus $h\nu$ (figure 6).

FIGURE 6: PLOTS OF $[\alpha(h\nu)]^2$ VERSUS THE PHOTON ENERGY $h\nu$

The calculated values of optical band gap E_g of tin doped NiO are summarized in table 4

TABLE 4: CALCULATED VALUES OF EG AND URBACH ENERGY E_U

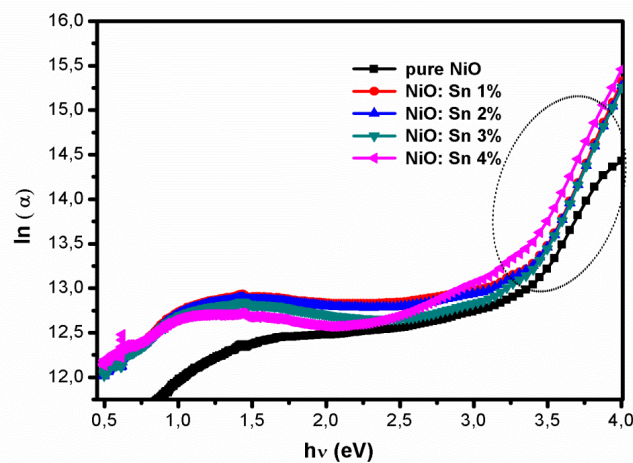
	E_g (eV)	E_U (meV)
Pure NiO	3.633	299.86
NiO: Sn 1%	3.590	294.68
NiO: Sn 2%	3.604	309.41
NiO: Sn 3%	3.609	405.56
NiO: Sn 4%	3.543	295.25

It is observed that the energy gap of the Sn-doped NiO thin films is lower than that of undoped NiO. This is consistent with the increase of the thin films which prepared transmittance.

The defects suggested above can be achieving a state density sprawl in the band gap; this effect can be interpreted by using the empirical Urbach law [46, 47]:

$$\alpha = \alpha_0 e^{\frac{h\nu}{E_U}} \quad (9)$$

Where E_U is the Urbach energy which is estimated from the slopes of $(\ln \alpha (v))$ versus energy $h\nu$ plots of the films (Figure 7). E_U values are given in Table 4. It is found that Urbach energy increases with the tin content in NiO excepting the doping 4%.

FIGURE 7: PLOTS OF $\ln(\alpha)$ VERSUS $h\nu$ OF FILMS

Moreover, the minimum of Urbach energy was obtained at 1% Sn doping level, this is consistent with the structural study which suggests a low defects for 1% Sn doping level with a minimum values of both dislocation density and compactness.

2) Opto-thermal Investigation

Opto-thermal properties of NiO: Sn thin films were investigated through The Amlouk–Boubaker opto-thermal expansivity Ψ_{AB} [48-50]. This parameter has been defined by equation (10)

$$\Psi_{AB} = \frac{D}{\hat{\alpha}} \quad (10)$$

Where D is the thermal diffusivity and $\hat{\alpha}$ is the effective absorptivity.

The effective absorptivity $\hat{\alpha}$ is defined as the mean normalized absorbance weighted by $I(\lambda)_{AM1.5}$, the solar standard irradiance, with λ : the normalised wavelength:

$$\hat{\alpha} = \frac{\int_{\lambda_{\min}}^{\lambda_{\max}} I(\lambda)_{AM1.5} \times \alpha(\lambda) d\lambda}{\int_{\lambda_{\min}}^{\lambda_{\max}} I(\lambda)_{AM1.5} d\lambda} \quad (11)$$

Where λ_{\min} and λ_{\max} are the limits of the visible spectrum and where $I(\lambda)_{AM1.5}$ is the Reference Solar Spectral Irradiance RSSI.

Table 5 summarizes the calculated values of Ψ_{AB} of NiO: Sn thin films. This result is in agreement with optical band gap described above. At this stage and regarding the variation of this parameter versus doping amount, minimum values of $\hat{\alpha}$ are obtained for 1% doping level. This doping level seems good for optoelectronic applications by reducing the absorption in solar cells using this doping material type. In correlation with both the optical and structural studies, 1% doping level has the minimum of defects. These defects were studied through the dislocation density in the structural section and Urbach energy in optical section.

TABLE 5: CALCULATED VALUES OF Ψ_{AB} OF NIO:SN SPRAY THIN FILMS

	NiO	NiO:Sn 1%	NiO:Sn 2%	NiO:Sn 3%	NiO:Sn 4%
$\Psi_{AB} (10^{-12} \text{m}^2 \text{s}^{-1})$	6,94	6,72	7,38	7,41	11,23

This effect is probably related to the difference of oxidation number of Ni (Ni^{2+}) and Sn (Sn^{2+} and Sn^{4+}). For 1% doping level is probably due to the decreases of the free charge carriers. For 2%, 3% and 4% doping level, it is possible to have some entities of tin oxide. These entities are not observed in XRD diagram because of the low doping level (less than 5%)

3) Refractive Index And Extinction Coefficient

Refractive index and the extinction coefficient of films have been calculated using optical experimental measurements by means of methods of Belgacem *et al.* [51]. The calculated variation of refractive index varying with the phonon energy for all films is shown in figure 8.

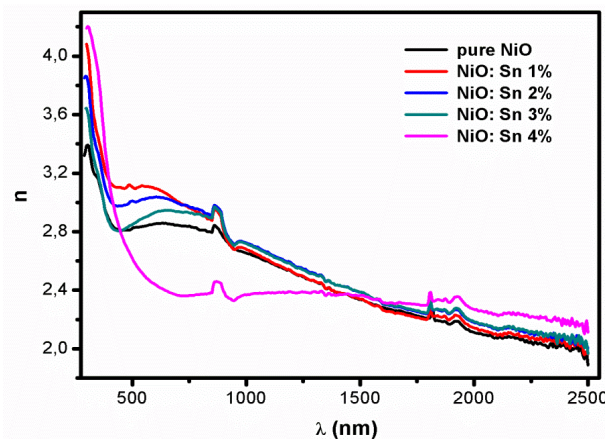


FIGURE 8: THE REFRACTIVE INDEX VARIATION VERSUS WAVELENGTH

For a given doping, we note a decrease of the refractive index values with the wavelength in the range [2.13; 3.15]

On the other hand, the refractive index n variation for all samples in the visible range obeys to Cauchy law [52]:

$$n = A + \frac{B}{\lambda^2} \quad (12)$$

Where: A and B are the Cauchy's parameters their values are listed in table 6.

TABLE 6: CALCULATED VALUES OF CAUCHY PARAMETERS A AND B

	A	B (μm^2)
Pure NiO	1,783	0,1544
NiO: Sn 1%	1,771	0,1788
NiO: Sn 2%	1,836	0,1522
NiO: Sn 3%	1,793	0,1855
NiO: Sn 4%	1,932	0,1952

The refractive index is found to increase with the increase of Sn concentration. Whereas the extinction coefficient of films is characterized by an increase but remains relatively low in the domain [0.012 ; 0.039] as shown in Figure 9. In fact, the slight increase in the values of k at the long wavelengths is due to the contribution of the absorption of the free carriers which is much stronger in the doped layers. Therefore, in the visible, the low value of k implies that these films are transparent as shown in the transmission spectra.

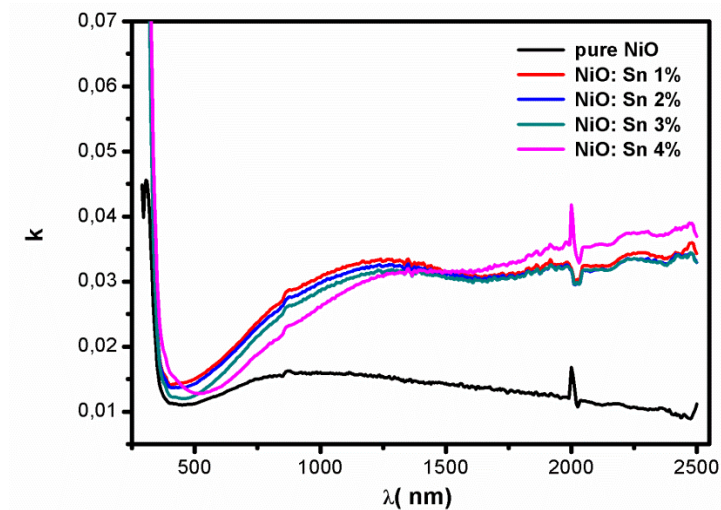


FIGURE 9: PLOTS OF THE EXTINCTION COEFFICIENT VERSUS WAVELENGTH

In addition, there is a change of type, this increase is due to an excess metallic suggesting the type n , doping Sn favors the passage of NiO from p -type to type n

From the refractive index and the extinction coefficient results, we have analyzed the real and imaginary parts of complex dielectric constant of pure and doped NiO with tin at different concentrations using the following relations [53, 54]:

$$\varepsilon(\lambda) = (n(\lambda) - ik(\lambda))^2 = \varepsilon_1(\lambda) - i\varepsilon_2(\lambda) \quad (13)$$

$$\varepsilon_1(\lambda) = n(\lambda)^2 - k(\lambda)^2 \quad (14)$$

$$\varepsilon_2(\lambda) = 2n(\lambda)k(\lambda) \quad (15)$$

For all samples, it is found that in infrared range the dispersion of $\varepsilon_1(\lambda)$ as linear function of the square of the wavelength λ^2 while the absorption $\varepsilon_2(\lambda)$ is linear with λ^3 , this behavior is in good agreement with the classical theory of the dielectric constant which was expressed by the following system in the near infrared [55]:

$$\varepsilon_1(\lambda) = \varepsilon_\infty - \frac{\varepsilon_\infty \omega_p^2}{4\pi^2 c^2} \lambda^2 \quad (16)$$

$$\text{And } \varepsilon_2(\lambda) = \frac{\varepsilon_\infty \omega_p^2}{8\pi^3 c^3 \tau} \lambda^3 \quad (17)$$

Where ε_∞ is the dielectric constant at high frequencies, ω_p the pulsation plasma and the relaxation time τ

Figure 10 shows the variation of ε_1 vs λ^2 and figures 11 shows the variation of ε_2 vs λ^3 :

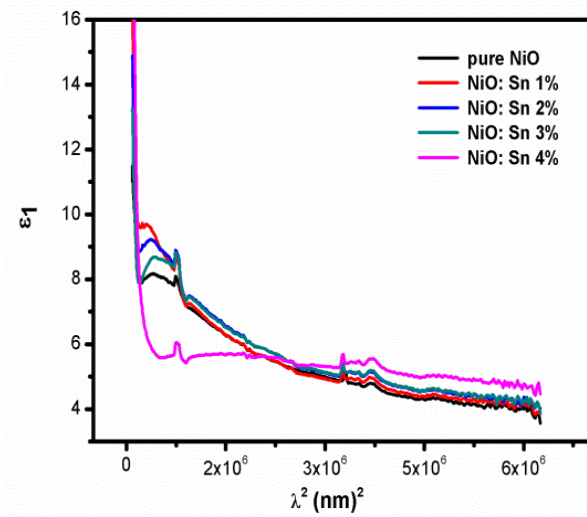


FIG. 10: E1 VERSUS λ^2

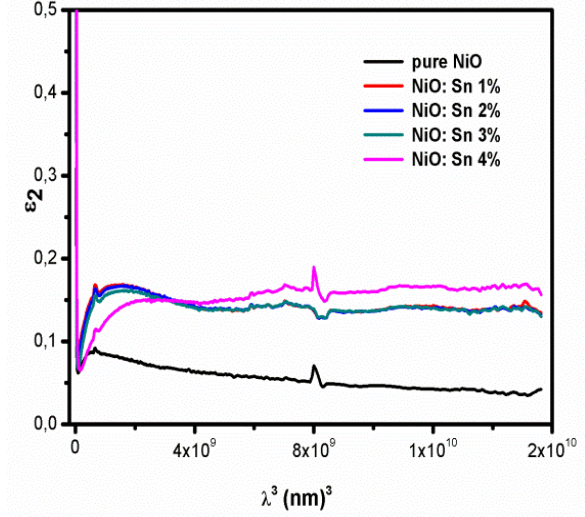


FIG. 11: E2 VERSUS λ^3

In the same line, the free carrier concentration to effective mass ratio $\frac{N}{m^*}$ is calculated from the following well-known equations [54]:

$$\omega_p^2 = \frac{4\pi N e^2}{\varepsilon_\infty m_e^*} \quad (18)$$

The calculated values of dielectric parameters are listed in table 7. It is found that ε_∞ which shows an increase from 5.42 to 6.10 is probably related to the increasing of free carried charge. Indeed, regarding the difference between the valence number of tin (IV +) and nickel (II +) the substitution of nickel element by tin element can increase the density of free charge.

TABLE 7: CALCULATED VALUES OF ε_0 , Ω_p AND OTHER CONSTANTS.

	ε_∞	ω_p ($10^{14} \text{ rad s}^{-1}$)	τ (10^{-13} s)	$\frac{N}{m^*}$ ($10^{17} \text{ g}^{-1} \text{ cm}^{-3}$)
Pure NiO	5,4242	-	-	-
NiO: Sn 1%	5,47855	3,87812	2,45102	2,84976
NiO: Sn 2%	5,83727	4,06953	3,67146	3,34348
NiO: Sn 3%	5,93254	4,13866	15,1687	3,51447
NiO: Sn 4%	6,10645	3,69225	1,2099	2,87919

PL Measurements

The effect of defects and quality of crystalline structure suggested above were highlighted via photoluminescence measurements using 270 nm excitation wavelengths. Figure 12 shows the PL spectra. The deconvoluted spectra (figure 13) show that PL response exhibits UV and violet emissions related to band to band transitions. It is found that pure NiO thin film displays a near band edge UV emission at 344 nm and shoulder peaks at 426, 452, 467 and 750 nm. The PL emission peaks are listed in table 8.

TABLE 8: THE POSITION OF EMISSION PEAKS.

NiO	1%	2%	3%	4%
344	346	344.5	345.5	347.5
426	380.5	398.5	397.5	361.5
452	399.5	420	425.5	389
467	425.5	426.5	460.5	399
750	466	455.5	515.5	425.5
	742	466	748	468
		753		759.5

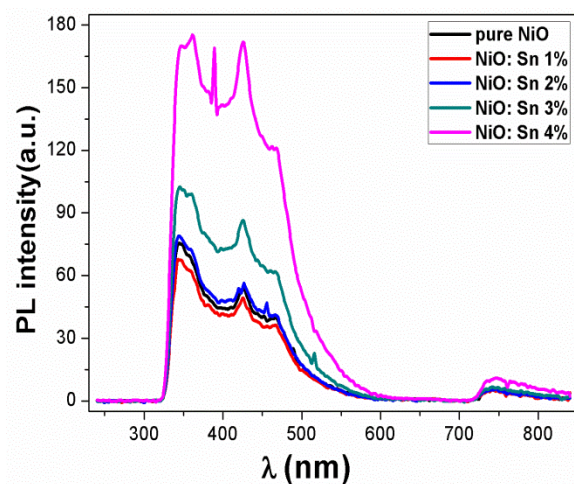
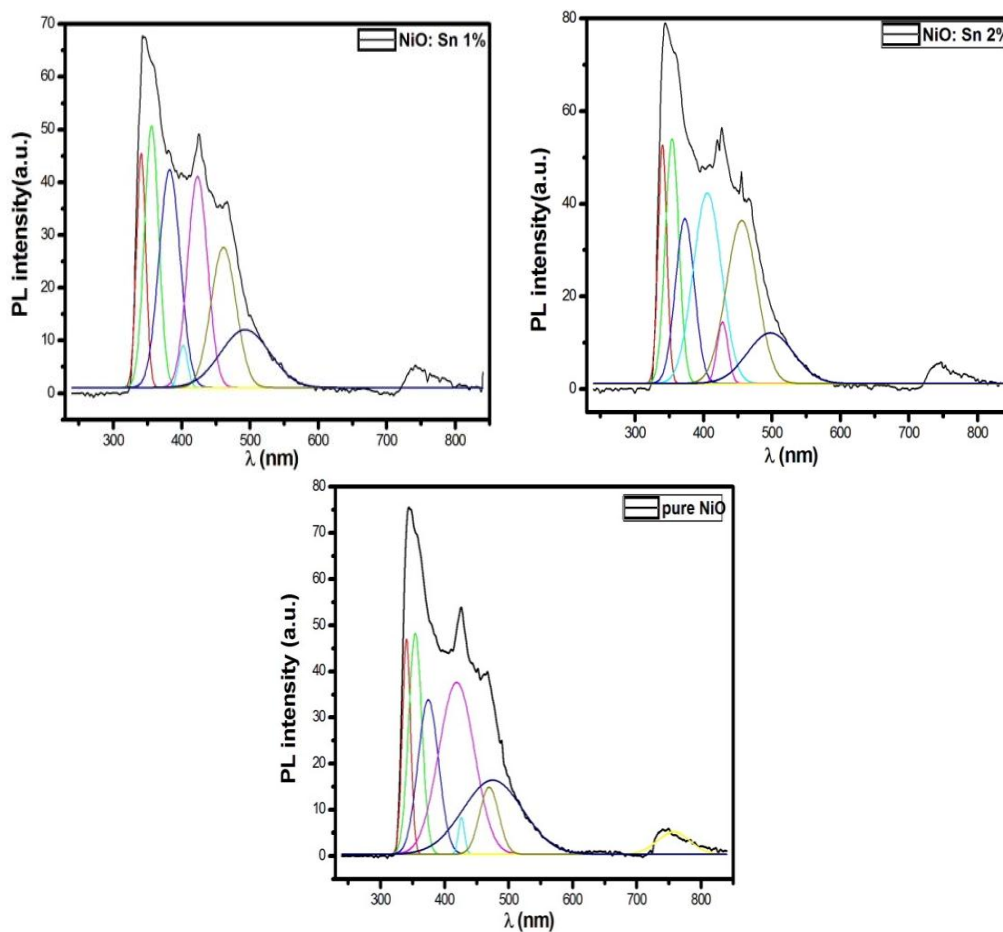


FIGURE 12: PL SPECTRA OF UNDOPED AND SN DOPED NIO THIN FILMS



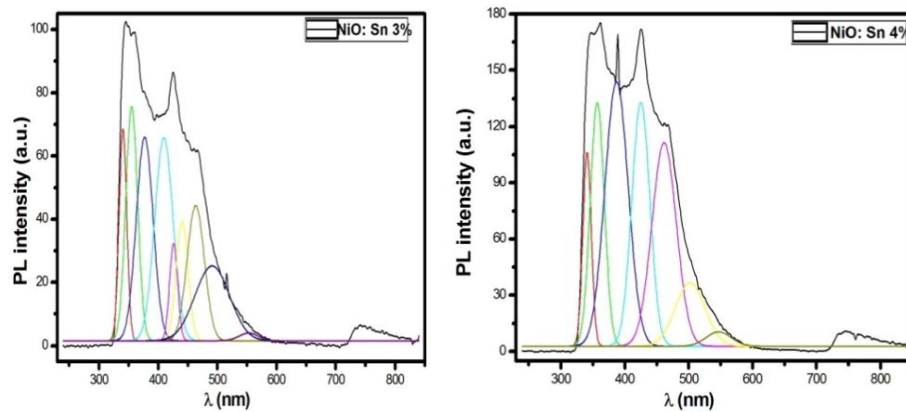


FIGURE 13: DECONVOLUTION OF PL SPECTRUM OF UNDOPED AND SN DOPED NIO THIN FILMS

The same behavior appears for both Sn doped NiO with a strongly response for 3% and 4% Sn doping level.

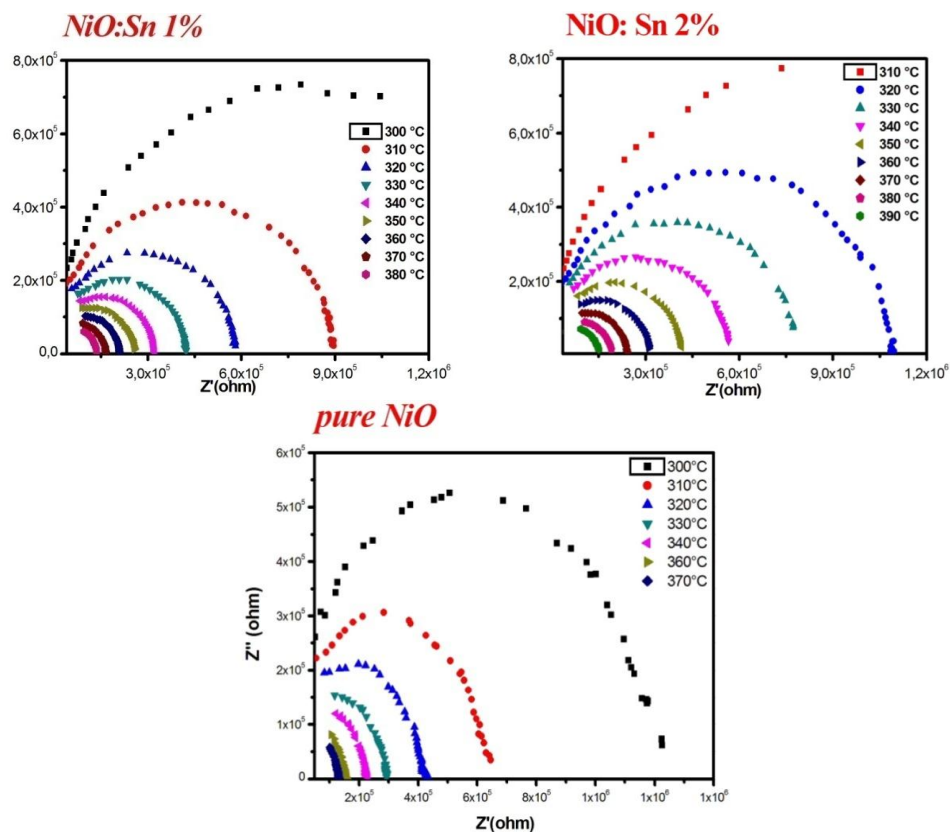
Besides, it is found that Sn doping reveals other luminescence peaks while retaining the strong emission. It is also found that 4% doping made except by promoting emission to 361 nm.

The peaks shift particularly of the strong one obtained in spectra PL can be linked to the variation of gap due to the incorporation of tin in NiO matrix. This incorporation can form others energy levels in the band gap which can explain the appearance of further peak.

The origin of the main strong peaks at 344nm and 361 nm for 4% was attributed to the electron transition of Ni^{2+} and O^{2-} ions which is also certified by the UV-vis absorption spectrum and which can be referred to the direct band transition. The shoulder emission peaks might be attributed to oxygen related defects (nickel vacancies).

Electrical Studies of Sn Doped Nio Thin Films

Figure 14 shows the typical complex impedance (Z'' versus Z') spectra of Sn doped NiO thin films in the temperature range for 300°C-410°C. The analysis of experimental data of all samples shows that the semi circles are depressed and their centers are shifted down to the real axis indicating distribution of relaxation.



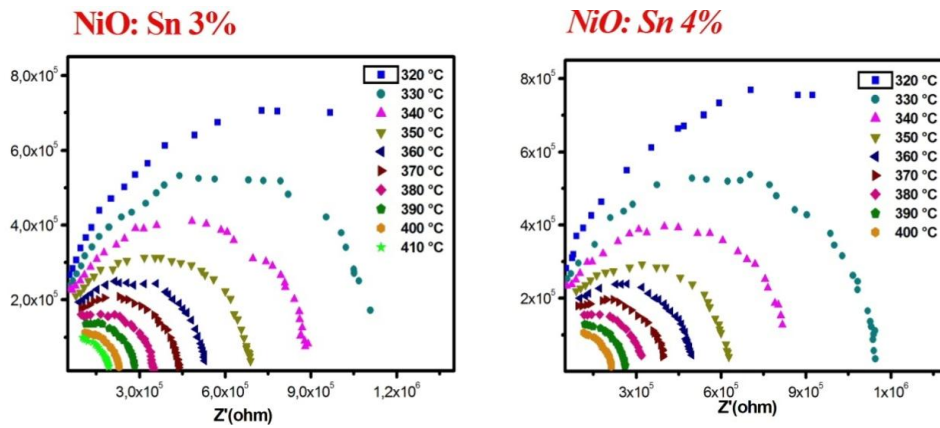
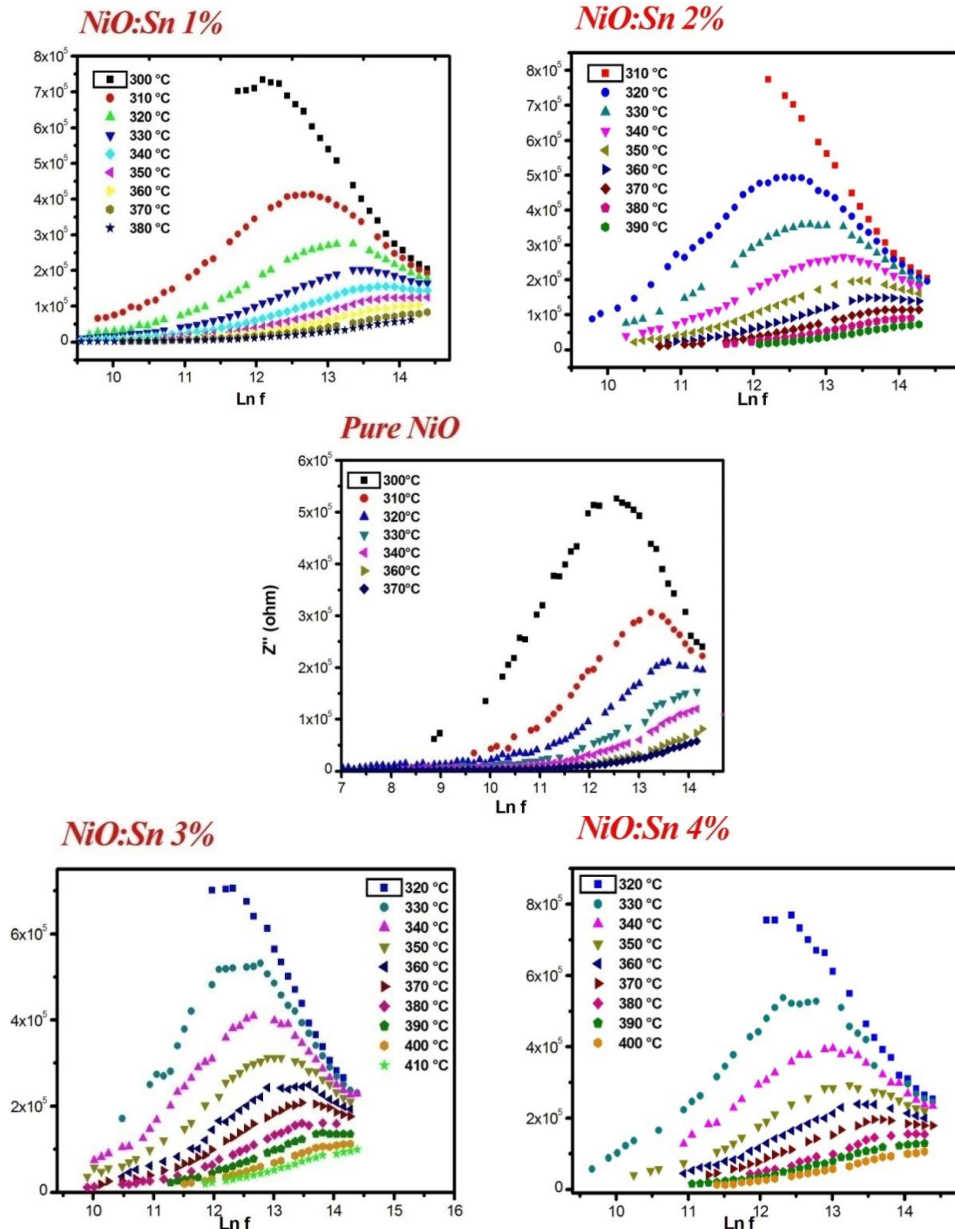
FIGURE14: COMPLEX IMPEDANCE SPECTRA (Z'' VERSUS Z') AT DIFFERENT TEMPERATURE.

Figure 15 shows Z'' versus frequency at different degrees of temperature, we observed that in Z''_{\max} peak shifts to higher frequencies with the change of temperature. This phenomenon reveals that the peak frequency indicates Arrhenius behavior and then we can determine the activation energy.

FIGURE 15: ANGULAR FREQUENCY DEPENDENCE OF Z'' AT DIFFERENT TEMPERATURES

In fact, the relaxation frequency obeys of these samples to Arrhenius law:

$$f_m = f_0 e^{\frac{-E_a}{kT}} \quad (19)$$

Where w_0 is a constant and E_a is the activation energy

As shown in figure 16, the expression of $\ln(f_m)$ versus $\frac{1000}{T}$ leads to a linear function which is a good agreement with expression. The calculated values of the activation energy for the samples of Sn doped NiO thin films are depicted in table 9.

TABLE 9: CALCULATED E_a VALUES OF RELAXATION FOR ALL SAMPLES.

sample	E_a (eV)
Pure NiO	0.3374
NiO: Sn 1%	1.0244
NiO: Sn 2%	1.0553
NiO: Sn 3%	0.9198
NiO: Sn 4%	1.0289

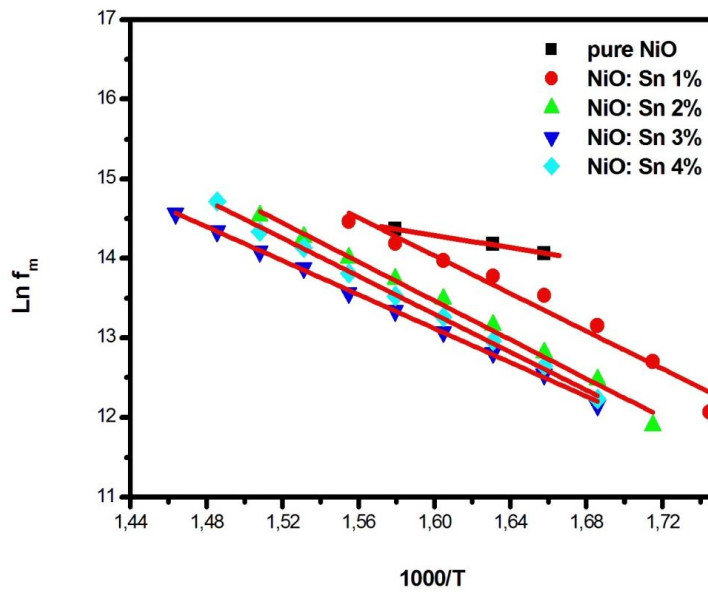


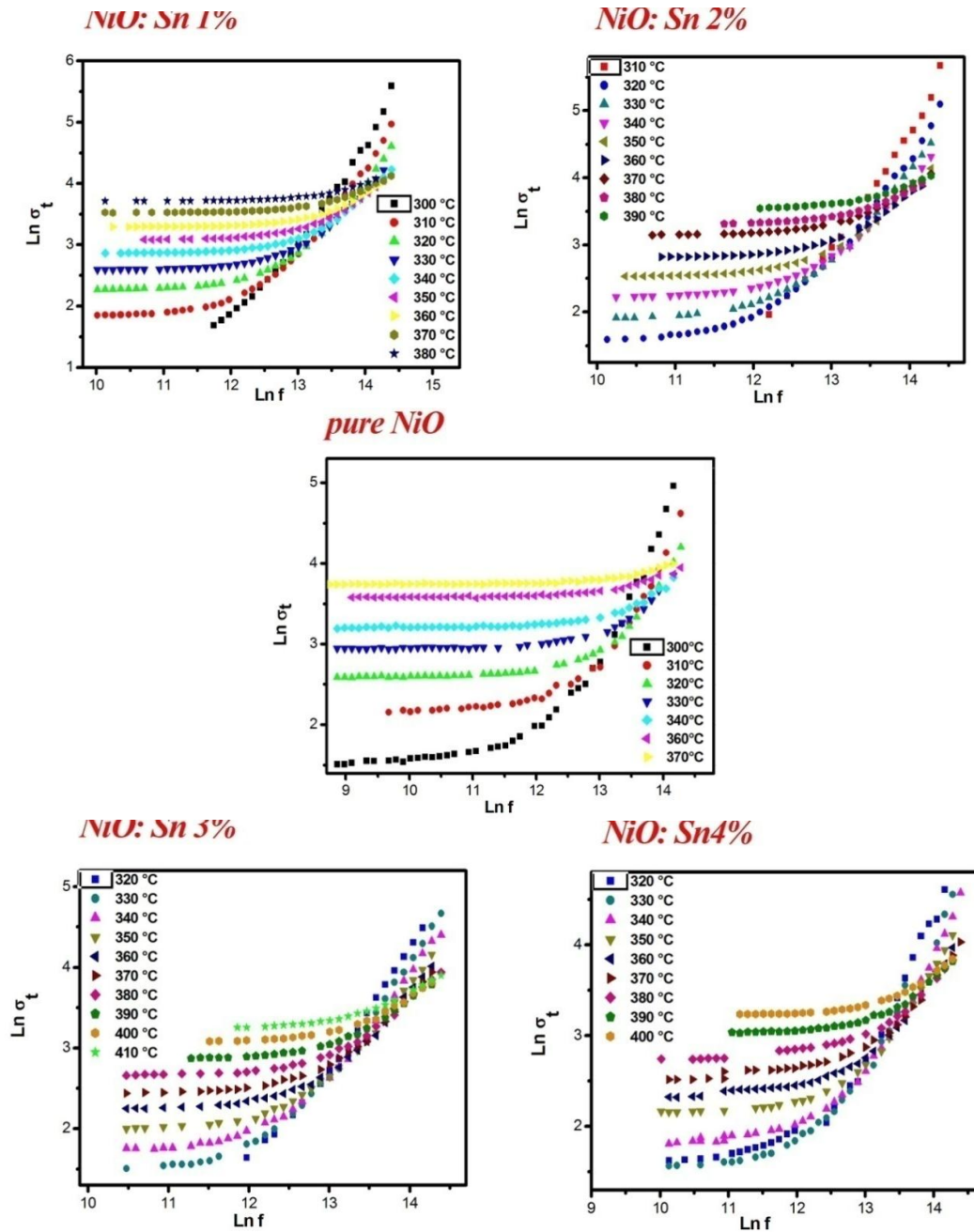
FIGURE 16: ANGULAR FREQUENCY RELAXATION AT DIFFERENT TEMPERATURE.

DC conduction studies provide an idea about the conduction of free charges under the application of an external electric field while AC conducting demonstrates the frequency depended conductivity, where the conduction occurs via trap levels situated between the band gaps of the materials. The ac conductivity σ_{ac} can be calculated using the relation [56] and [57]

$$\sigma_{ac} = \sigma_{dc} \left[1 + \left(\frac{\omega}{\omega_0} \right)^s \right] \quad (20)$$

where (σ_{DC}) is the dc conductivity obtained from the extrapolation to zero frequency of the $\ln(\sigma_{ac})$ versus $\ln(f)$ curves, ω_0 is the hopping frequency of the charge carriers, where $\sigma_{ac}(\omega_0) = 2\sigma_{dc}(0)$, and s is the frequency exponent.

Figure 17 shows a representative example for the relation between $\ln\sigma_i$ and $\ln f$ for Sn doped NiO films at different temperatures.

FIGURE 17: FREQUENCY DEPENDENCE OF AC CONDUCTIVITY $\Sigma_{AC}(\Omega)$ DIFFERENT TEMPERATURE

It is clear that $\text{Ln}\sigma_{ac}$ increases with increasing frequency according to equation precedent. The values of the frequency exponent s were calculated for all the investigated samples at different temperatures from the slope of the linear lines of $\text{Ln}\sigma_t$ vs $\text{Ln}f$. The temperature dependence of the mean values of s for these films is shown in figure 18; it is found that s has value ≤ 1 and decreases as the temperatures increases suggesting a hopping conduction mechanism i.e. which is consistent with the correlated barrier hopping (CBH) model [57]. In this model, the angular frequency exponent s is linked to the temperature through the expression:

$$s = 1 - \frac{6kT}{W_m} \quad (21)$$

Where k is the Boltzmann constant, T is the temperature and W_m is the polaron binding energy.

Values of W_m can be calculated from Eq.21. Table 10 illustrates the values of W_m . It is observed that W_m has an irregular variation with Sn content. This may be related to both substitution of nickel by tin element and formation of SnO_2 entities which are not observed by XRD analysis due to the low Sn content ($\frac{[\text{Sn}]}{[\text{Ni}]} < 5\%$)

TABLE 10: CALCULATED VALUES OF W_m FOR ALL SAMPLES

	W_m (eV)
Pure NiO	2.4642
NiO: Sn 1%	1.398648
NiO: Sn 2%	1.784482
NiO: Sn 3%	1.669354
NiO: Sn 4%	1,617,187

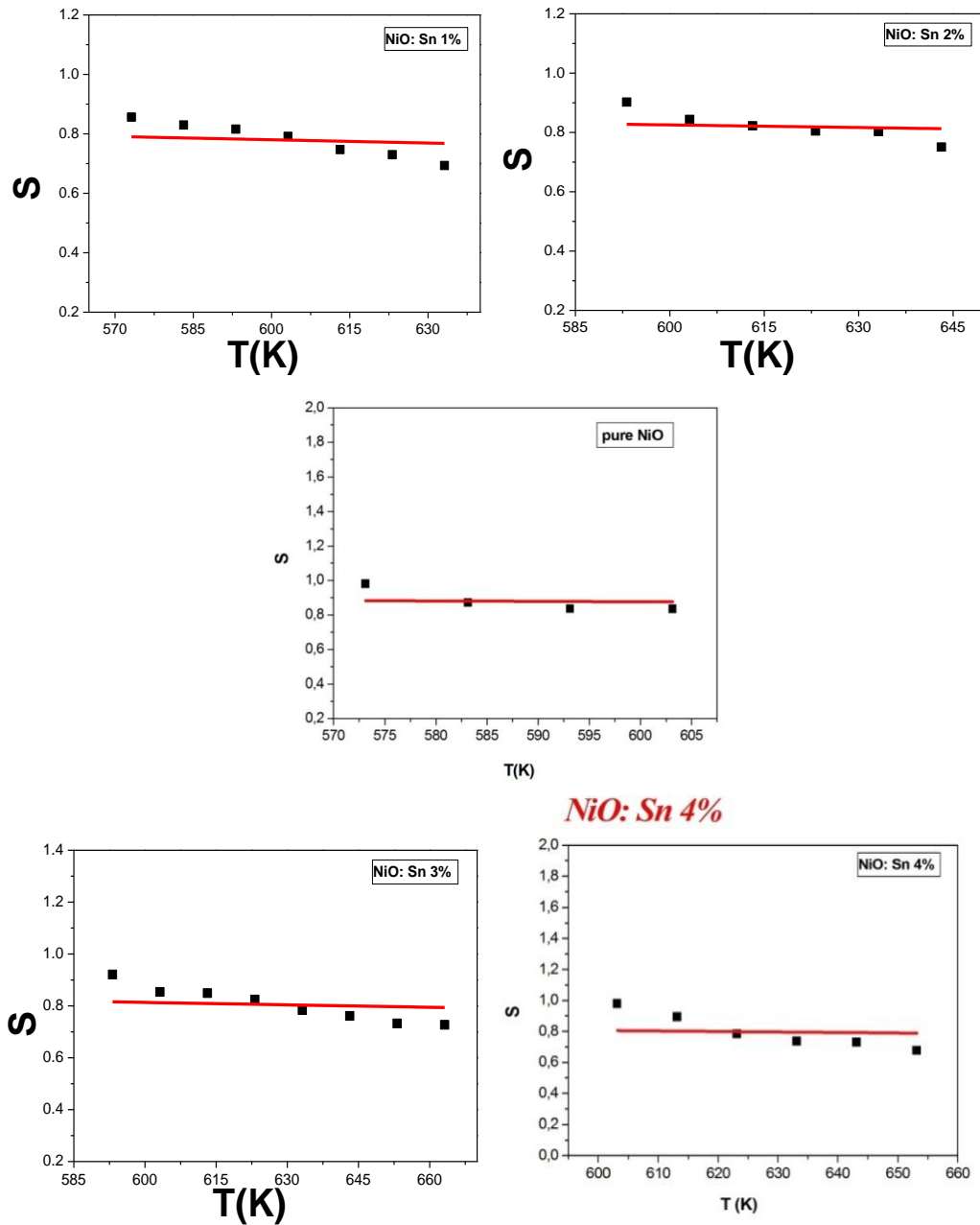


FIGURE 18: TEMPERATURE DEPENDENCE OF THE ANGULAR FREQUENCY EXPONENTS

Moreover, in the range of temperature measurements, all the data points give a straight line according to Arrhenius law [58]

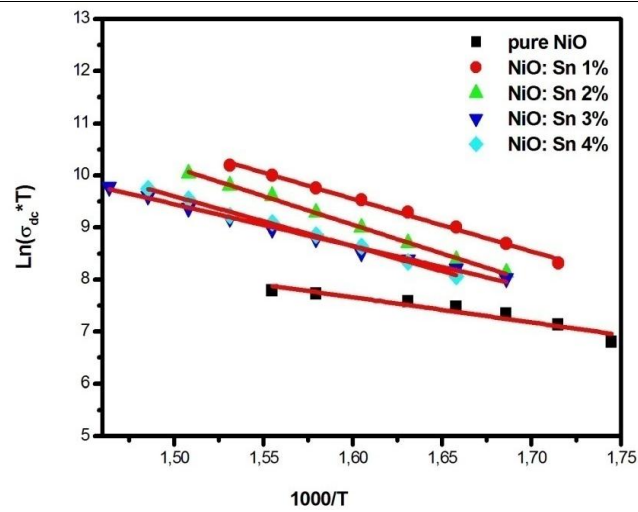
$$\sigma_{dc} = \frac{A}{T} \exp\left(\frac{-E_a}{kT}\right) \quad (22)$$

Where A is a constant and E_a is the activation energy.

Figure 19 shows the variation of $\ln(\sigma T)$ Vs $1000/T$. This variation is consistent with Arrhenius law. The activation energy values related to electrical conductivity are given in table 11. It is found that the values of E_a are Convergent and almost identical to the activation energy obtained from the angular relaxation frequency suggesting a hopping mechanism.

TABLE 11: VALUES OF EA

sample	E_a (eV)
Pure NiO	0.4167
NiO: Sn 1%	0.8701
NiO: Sn 2%	0.9498
NiO: Sn 3%	0.69277
NiO: Sn 4%	0.8277

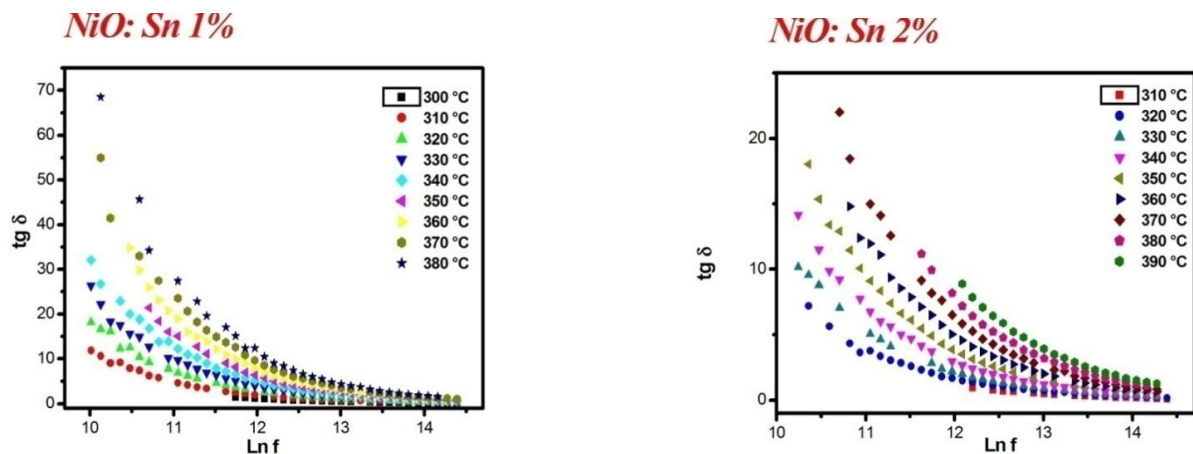
FIG. 19: LN ($\Sigma_{dc} * T$) VERSUS $1000/T$

From these electric measurements, some dielectric parameters were also investigated.

First, dielectric loss tangent ($\tan(\delta)$) is an important source of formation in thin films. This parameter can be used to reach the electrical and dipolar relaxation time and its activation energy. It is expressed as [27, 59, 60, 61]:

$$\tan \delta = \frac{Z_1}{Z_2} \quad (23)$$

It is found that this parameter decreases with frequency and increases rather with temperature (figure 20). Since the exchange energy is linked to Z_1 , this behavior indicates that these uncross losses with frequency and increase with temperature. In addition, the dipole interaction is as an orientation bias therefore decreases with temperature according to Curie law.



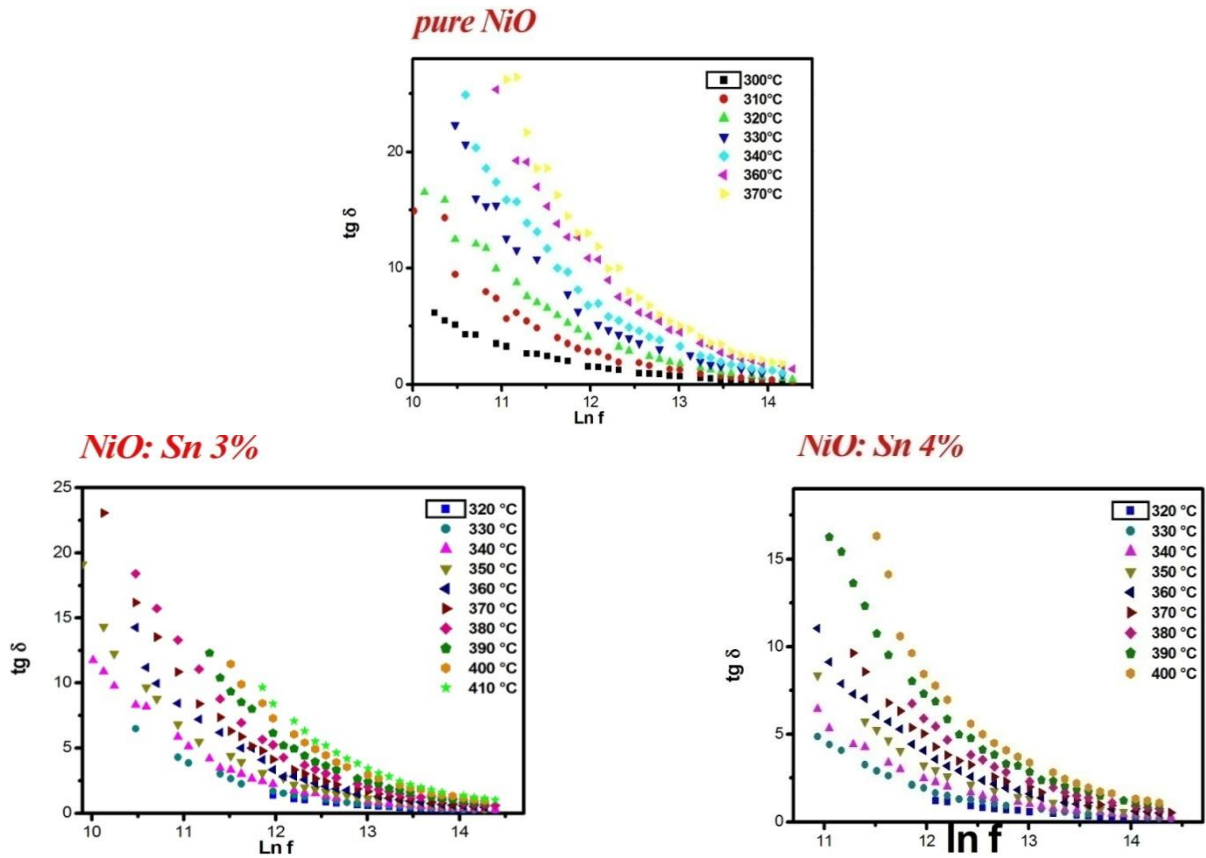


FIGURE 20: VARIATION OF TAN Δ AT DIFFERENT TEMPERATURES.

Indeed, when an electric field is applied to these materials, there occurs a phenomenon of dielectric polarization or dipole, that is to say, the dipole moment is oriented with the field. In such materials, the "dielectric loss", is a phase difference between the electric field and the dipole polarization. Relaxation, resulting, converts a portion of the electromagnetic energy into thermal energy.

The energy dissipated in the object is given by the following equation: [62]

$$P = \iiint_{\text{material}} \varepsilon_2 \omega |E|^2 dV \quad (24)$$

Where ω is the angular frequency, ε_2 imaginary part of the dielectric permittivity and E is the electric field. It is noted that the dielectric loss changes with temperature [63]. Indeed, the thermal agitation is originally s changes degrees of order of the material. This order can be of different types: order between different cations, order of magnetic moments and order of dipole moment. This effect was observed by M.E. Lines and A. M. Glass in KH_2PO_4 [64]

Furthermore, the dielectric response can be described by expression of the complex relative dielectric constant as an amount consists of a real part and an imaginary component is expressed as:

$$\varepsilon(\omega) = \varepsilon_1(\omega) - i\varepsilon_2(\omega) \quad (25)$$

Where ε_1 and ε_2 are respectively the real and imaginary part of dielectric constant, representing the amount of energy stored in a dielectric material as polarization and the energy lose, while applying an electric field.

In addition, the conductivity σ_{ac} originates from the bound and free charges and can be expressed in terms of the absolute permittivity ε_0 and the dissipation:

$$\sigma_{ac} = \varepsilon_0 \omega \varepsilon_2(\omega) \quad (26)$$

$$\sigma_{ac} = \varepsilon_0 \varepsilon_1(\omega) \omega \tan(\delta) \quad (27)$$

The variations of the real part of dielectric constant, $\epsilon_1(\omega)$ with the frequency at different temperature of NiO doped Sn thin films are shown in figure 21. It can be seen that $\epsilon_2(\omega)$ decreases with increasing frequency and increases with the increase of temperature (figure 22). So, these prepared thin films possess high dielectric constant, making these compounds potential candidate for super-capacitor applications.

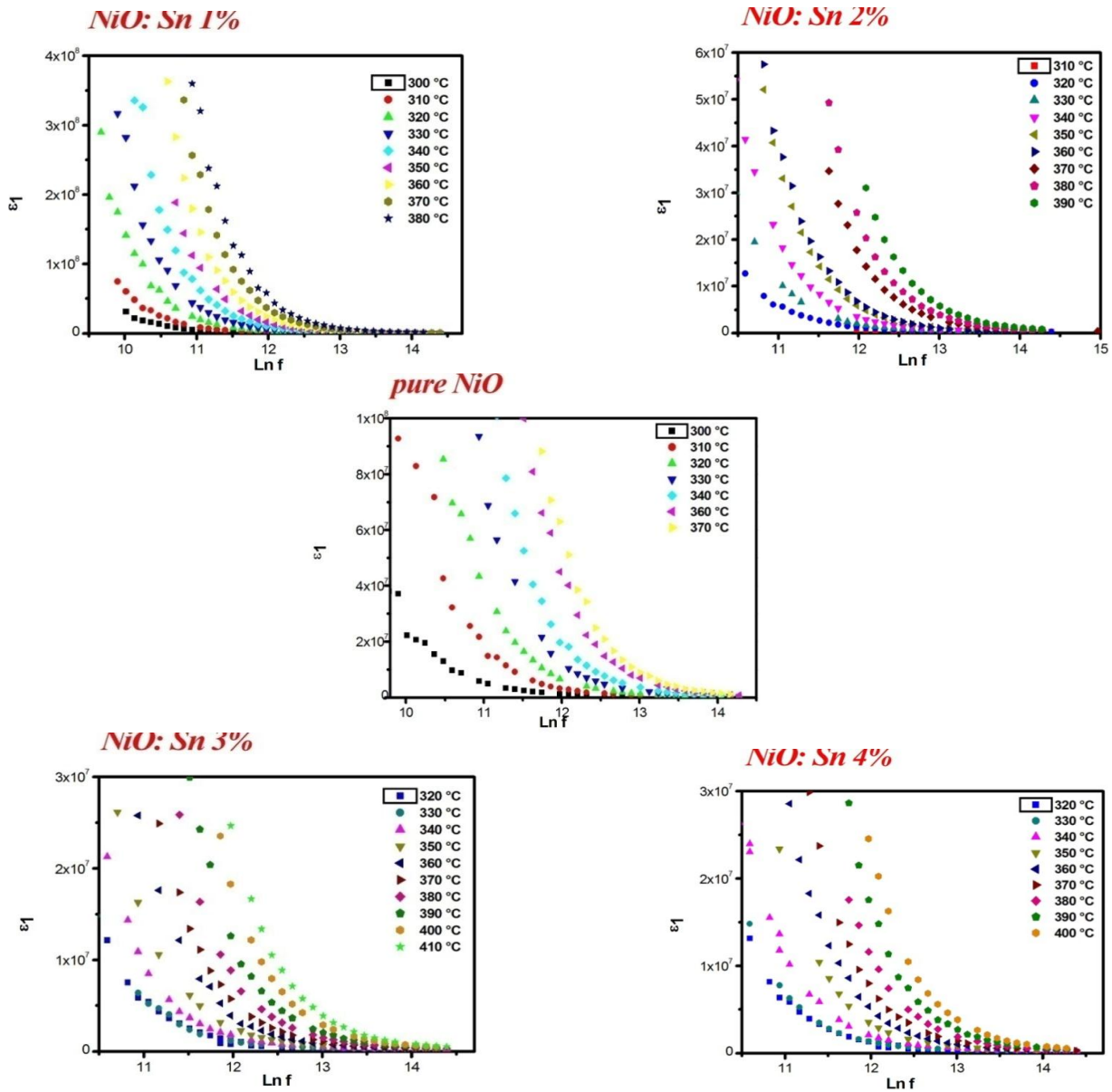
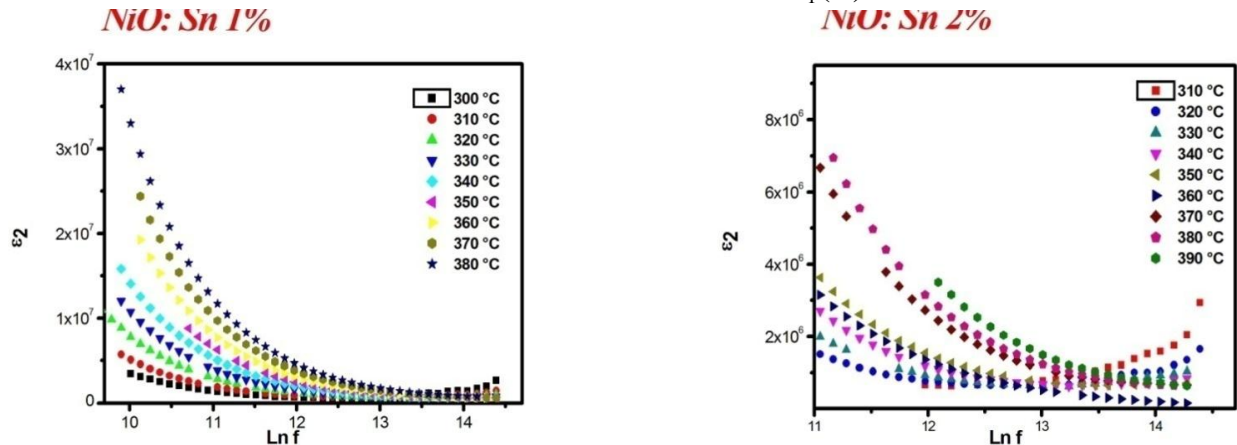
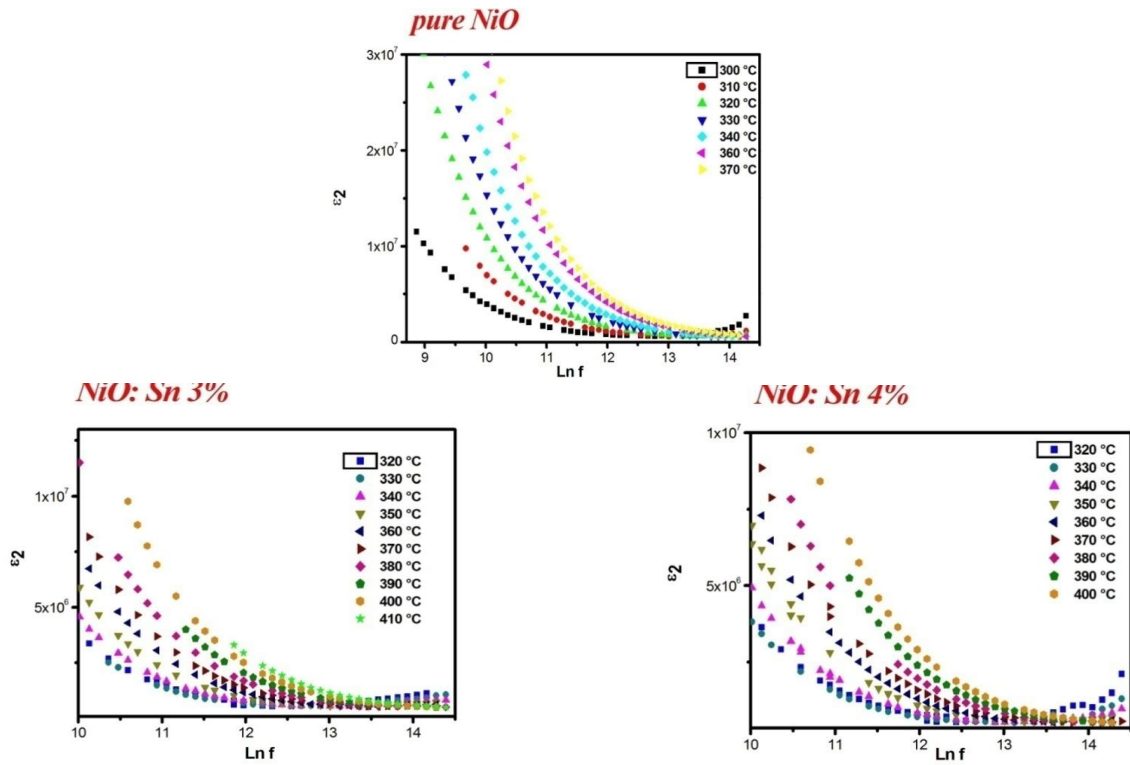
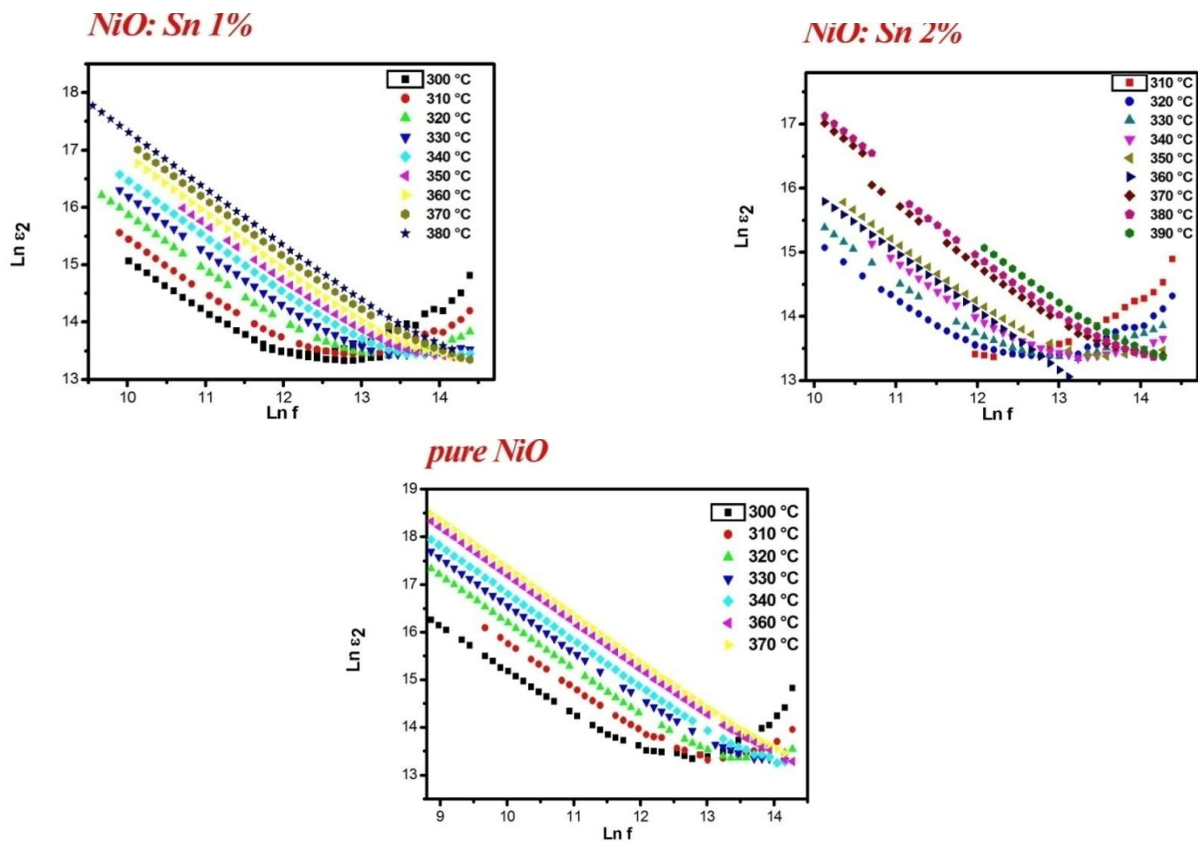


FIGURE 21: FREQUENCY DEPENDENCE OF THE DIELECTRIC CONSTANT $\epsilon_1(\omega)$ AT DIFFERENT TEMPERATURES.



FIGURE 22: FREQUENCY DEPENDENCE OF THE DIELECTRIC CONSTANT $\epsilon_2(\omega)$ AT DIFFERENT TEMPERATURES.

In the same line, the dependence of the imaginary part of the dielectric constant, $\epsilon_2(\omega)$ on the frequency at different temperatures of NiO doped Sn thin films is illustrated in Figure 23, as observed, $\epsilon_2(\omega)$ decreases on increasing frequency and increases with increasing temperature. This decrease consists of two contributions: one from the DC conduction at low frequency and the other from the dielectric polarization processes at high frequency.



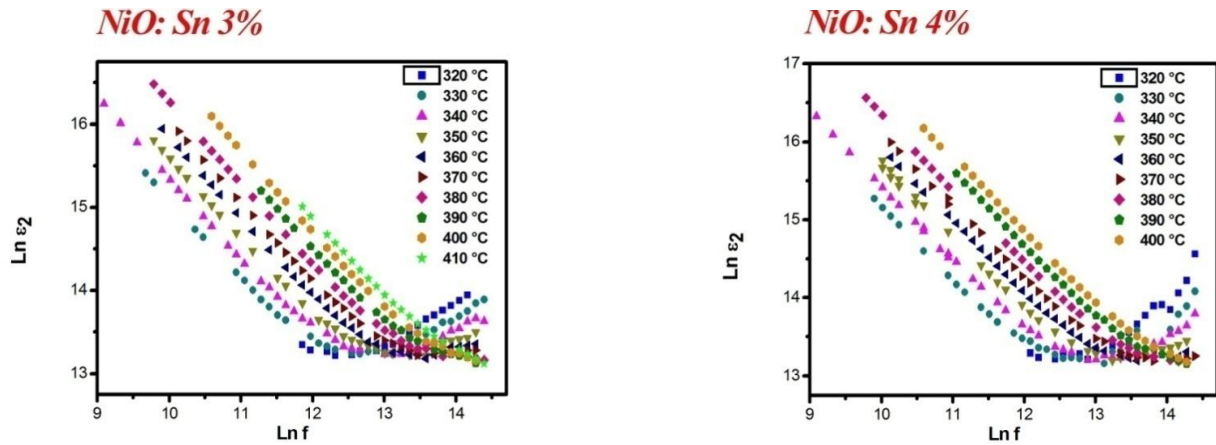


FIGURE 23: FREQUENCY DEPENDENCE OF THE DIELECTRIC CONSTANT $Ln\epsilon_2(\omega)$ AT DIFFERENT TEMPERATURES.

Discussion of Sn Doped NiO Thin Films Growth Patterns in Terms of the LCT

Since X-Ray Diffraction spectra and lattice parameter calculation (§3.1 and §3.3.1) evoked the dynamics of a possible Sn incorporation inside the nickel oxide thin films. Crystalline size evaluation revealed that tin has a relative tendency to form Sn_xO_y crystalline phases. At this level, the recently proposed Lattice Compatibility Theory [65-75] which was implied in similar cases, has been evoked. This theory, as mentioned in some recent studies [66-74] has been based on the interaction of doping-element lattice behavior versus host edifice.

Fundamentals to the Lattice Compatibility Theory [65-75] have been established by Petkova *et al.* [65] in a study of Urbach tailing controversial behaviour in some nano-compounds as well as I-III-O₂ ternary oxides instability at low temperatures. Elements of the Lattice Compatibility Theory have been presented later by Colantoni *et al.* [66] Yumak *et al.* [67], Ben Said *et al.* [68], Gherouel *et al.* [69], Haj Lakhdar *et al.* [70], Boubaker *et al.* [71-73], Ben Messaoud *et al.* [74] and Mimouni *et al.* [75].

Elements from this theory refer mainly to bonds and geometrical compatibility patterns between a final structure of a given element and those of its intrinsic lattice as-native in the nature. They give hence plausible explanations [66-69] to the comparative stability of some lattice structures.

In this study (Sn-doped NiO thin films), the Lattice Compatibility Theory can give a plausible understanding of the disparity concerning doping element incorporating dynamics starting from intrinsic doping-element lattice properties in comparison to those of the host. Calculation of Sn_xO_y thin films relevant parameters (Fig. 24) led to the conviction that the lack of compatibility with NiO host crystalline structure is not favorable to the growth of any stable NiO: Sn thin films, merely for high doping amounts, which has been recorded earlier.

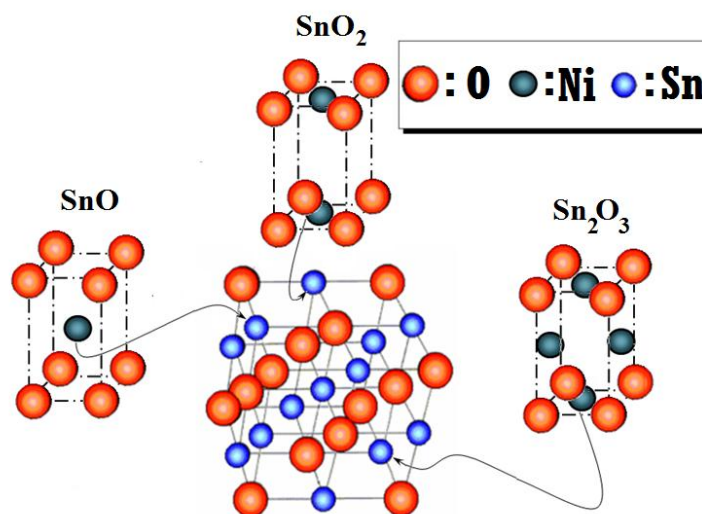


FIGURE 24: NIO CRYSTAL ELEMENTARY LATTICE AND Sn_xO_y DOMINANT THIN FILMS STRUCTURES (A,B,C).

In fact, this particular behavior of tin atoms within targeted lattices has been evoked in materials chemistry and physics fields by Bougrine *et al.* [76], Ghimbeu *et al.* [77], Jiménez *et al.* [78] in the cases of spray pyrolysis-prepared ZnO films, electrostatic-sprayed indium oxide and co-doped barium-phosphate glasses, respectively.

Conclusion

In this work, we have reported some physical properties related to nickel oxide in terms of tin doping level. Indeed, Sn-doped NiO thin films with different tin content have been successfully synthesized by using low cost spray pyrolysis technique at 460°C on glass substrate. These prepared films with cubic structure have a high crystalline quality with the (111) preferred orientation. The PL spectra exhibit UV and violet emission related to band to band transitions with increasing of doping. The optical transmission spectra exhibited a high percentage transmittance in the visible regime. The optical band gap has been found to decrease from 3.63 to 3.54 eV with Sn content.

Finally, the DC conductivity shows an increasing tendency with the increase of temperature which indicates a thermally activate phenomenon. The activation energy obtained from both angular relaxation frequency and dc conductivity suggests that the carrier transport mechanism is a hopping mechanism thermally activated in the band gap. Also, electric measurements show that AC conductivity is consistent with model of correlated barrier hopping (CBH). Maximum barrier height W_m is in good agreement with CBH theory. This result is very interesting; since the use of low-cost and simple spray pyrolysis technique has been used to prepare such oxide and open the way for the possible application of prepared films in various optoelectronic devices. Further study is in progress to reach some tests and the magnetic properties of these doped films.

ACKNOWLEDGMENT

The corresponding author, Pr. Dr. Ing. Karem Boubaker, would express here, on behalf of all the authors, particular gratefulness's to H. E. KRASSIMIR PETROV, Plenipotentiary Minister, with all his honourable staff within the Bulgarian embassy in Tunis, for helpfulness and moral supply. Particular thanks are also addressed H. E. ÖMER GÜCÜK, the Turkish Ambassador in Tunisia, along with his colleagues, mainly Mr. EROL TORAMAN and Mr. ÜMIT ÖKTEM, for encouragement and help.

REFERENCES

- [1] S.C. Chen, T.Y. Kuo, Y.C. Lin, H.C. Lin, *Thin Solid Films*, 519 (2011) 4944.
- [2] H. Sato, T. Minami, S. Takata and T. Yamada, *Thin Solid Films*, 236 (1993) 27.
- [3] T. Sunde, M. Einarsrud, T. Grande, *Thin Solid Films*, 573 (2014) 48.
- [4] M. Matsumiya, F. Qiu, W. Shin, N. Izu, N. Murayama, S. Kanzaki, *Thin Solid Films*, 419 (2002) 213.
- [5] A.Saleh, *International Journal of Application or Innovation in Engineering & Management*, 2(2013)2319.
- [6] S. Thota, J. H. Shim, and M. S. Seehra, *J. of Applied Physics*, 114(2013), 214307.
- [7] S. Guo, W. Liu, X. H. Liu, W. J. Gong, J. N. Feng, Z.D.Zhang *Journal of Magnetism and Magnetic Materials* 324 (2012) 3933.
- [8] S.S. Nkosi, B. Yalisi, D.E. Motaung, J. Kearthland, E. Sideras-Haddadb, A. Forbes, B.W. Mwakikung, *Applied Surface Science*, 265 (2013) 860.
- [9] S. Pereira, A. Gonçalves, N. Correia, J. Pinto, L. Pereira, R. Martins, E. Fortunato, *Solar Energy Materials and Solar Cells*, 120 (2014) 109.
- [10] H. Moulki, C. Faure, M. Mihelčič, A. Šurca Vuk, F. Švegl, B. Orel, G. Campet, M. Alfredsson, A.V. Chadwick, D. Gianolio, A. Rougier, *Thin Solid Films*, 553 (2014) 63.
- [11] G. Bodurov, P. Stefechev, T. Ivanova, K. Gesheva, *Materials Letters*, 117 (2014) 270.
- [12] J. Warnan, Y. Pellegrin, E. Blart, L. Zhang, A. Brown, L. Hammarström, D. Jacquemin, F. Odobel, *Dyes and Pigments*, 105 (2014) 174.
- [13] A. Echresh, Ch. Oeurn Chey, M. Zargar Shoushtari, V. Khranovskyy, O. Nur, M. Willander, *Journal of Alloys and Compounds* 632(2015) 165.

- [14] V.S. Vaishnav, S.G. Patel, J.N. Panchal, *Sensors and Actuators B: Chemical* 210(2015), 165.
- [15] N.S. Das, B.Saha, R.Thapa, G.C.Das, K.K.Chattopadhyay, *Physica E*, 42 (2010) 1377.
- [16] P. Chou, H. Chen, I. Liu, C. Chen, J.Liou, K.Hsu, W.Liu, *International Journal of Hydrogen Energy*, 40 (2015) 729.
- [17] I. Gardunõ-Wilches, J.C. Alonso, *International journal of hydrogen energy*, 38 (2013) 4213.
- [18] Y. Ashok Kumar Reddy, A. Sivasankar Reddy, P. Sreedhara Reddy, *Journal of Alloys and Compounds*, 583 (2014) 396.
- [19] S.C. Chen, C.K. Wen, T.Y. Kuo, W.C. Peng, H.C. Lin, *Thin Solid Films*, 572 (2014) 51.
- [20] G. Turgut, E. Sonmez, S. Duman , *Ceramics International*, 41(2015) 2976.
- [21] Y. Wang, F. Zhang, L. Wei, G. Li, W. Zhang, *Physica B*, 457 (2015) 194.
- [22] V. Verma, M.Katiyar, *Thin Solid Films*, 527 (2013) 369.
- [23] R. Lo Nigro, S. Battiato, G. Greco, P. Fiorenza, F. Roccaforte , G. Malandrino, *Thin Solid Films*, 563 (2014) 50.
- [24] M. A. Mat-Teridi, A. A. Tahir, S. Senthilarasu, K. G. U. Wijayantha, M. Y. Sulaiman, N. Ahmad-Ludin, M. A. Ibrahim and K. Sopian, *Physica Status Solidi - Rapid Research Letters* , 8(2014) 982.
- [25] V. Gowthami, P. Perumal, R. Sivakumar, C.Sanjeeviraja, *Physica B*, 452(2014)1.
- [26] R. Sharma, A.D. Acharya, S.B. Shrivastava, T. Shripathi, V. Ganesan, *Optik*, 125 (2014) 6751.
- [27] M. Ben Amor, A. Boukhachem, K. Boubaker, M. Amlouk, *Materials Science in Semiconductor Processing* ,27 (2014) 994.
- [28] A. Boukhachem, R. Boughalmi, M. Karyaoui, A Mhamdi, R. Chtourou, K. Boubaker, M. Amlouk, *Materials Science and Engineering: B*, 188(2014) 72.
- [29] B.A. Reguig, A. Khelil, L. Cattin, M. Morsli, J.C. Bernede, *Applied Surface Science*, 253 (2007) 4330.
- [30] S. Moghe, A.D. Acharya, R. Panda, S.B. Shrivastava, M. Gangrade ,T. Shripathi, V. Ganesan, *Renewable Energy*, 46 (2012) 43.
- [31] L. Zhao, G. Su, W. Liu, L. Cao, J. Wang, Z. Dong, M. Song, *Applied Surface Science*, 257 (2011) 3974.
- [32] S. Kerli, U. Alver, H. Yaykasli, *Applied Surface Science* 318 (2014) 164.
- [33] W.Jang, Y.Lu, W. Hwang, W. Chen, *Journal of the European Ceramic Society*, 30 (2010) 503.. Yang, H.
- [34] M Pu, Q. Zhou, Q. Zhan , *Thin Solid Films*, 520 (2012) 5884.
- [35] K. Boubaker, *Materials Science and Engineering A*, 528 (2011) 1455.
- [36] P. Scherrer, *Nachr. Ges.Wiss.Göttingen*, 26 (1918) 98.
- [37] J.I. Langford and A.J.C. Wilson, *J. Appl. Cryst.* 11 (1978) 102.
- [38] S. Sen, S. K. Halder, S. P. Sen Gupta, *J. Phys. Soc. Jpn.* 38 (1975) 1641.
- [39] I. Hotový, J. Huran, J. Janík, A.P. Kobzev, *Vacuum*. 51 (1998), 157.
- [40] W. Jang, Y. Lu, W. Hwang, T. Hsiung, H.P. Wang, *Surface and Coatings Technology*.202 (2008), 5444.
- [41] M. Ristova, Y. Kuo and S. Lee, *Semicond. Sci. Technol*, 18 (2003) 788.
- [42] X.Y. Li, H.J. Li, Z.J.Wang, H. Xia, Z.Y. Xiong, J.X.Wang, B.C. Yang, *Opt. Commun.* 282(2009) 247.
- [43] A. Mhamdi, A. Boukhachem, M. Madani, H. Lachheb, K. Boubaker, A. Amlouk, M. Amlouk , *Optik* 124 (2013) 3764.
- [44] A. Boukhachem, C. Bouzidib, R. Boughalm , R. Ouertenic , M. Kahlaoui , B. Ouni , H. Elhouichet , M. Amlouk, *Ceramics International* 40 (2014) 13427.
- [45] R. Boughalmi, A. Boukhachem, M. Amlouk, *Materials Science in Semiconductor Processing* 30 (2015) 218.
- [46] F. Urbach, *Phys. Rev.* 92 (1953) 1324.
- [47] W. Martienssen, *J. Phys. Chem. Solids* 2 (1957) 257.
- [48] A. Amlouk, K. Boubaker, M. Amlouk, *J. Alloys Compd.* 490 (2010) 602.
- [50] A. Amlouk, K. Boubaker, M. Amlouk, M. Bouhafs, *J. Alloys Compd.* 485 (2009) 887.
- [51] S. Belgacem et R. Bennaceur, *Rev. Phys. Appl*, 25 (1990)1245.
- [52] H.G. Tompkins, W.A. McGahan. John Wiley & Sons Inc., New York, (1999)
- [53] M. Sesha Reddy, K.T. Ramakrishna Reddy, B.S. Naidu, P.J. Reddy, *Optical Materials* 4 (1995) 787.

- [54] J.I. Pankove , Prentice-Hall, New Jersey (1971) 92.
- [55] A.K. Wolaton, T.S. Moss, Proc. R. Soc. A 81 (1963) 5091.
- [56] A. K. Jonscher, Nature 267(1977) 673.
- [57] G. E. Pike, Physical Review B 6 (1972) 1572.
- [58] T. Larbi, B. Ouni, A. Boukhachem, K. Boubaker, M. Amlouk , Mater. Res. Bull.,60 (2014) 45.
- [59] B. Ouni, M. Haj Lakhdar, R. Boughalmi, T. Larbi, A. Boukhachem, A. Madani, K. Boubaker, M. Amlouk, Journal of Non-Crystalline Solids, 367(2013)) 1.
- [60] A. Boukhachem, A. Yumak S. Krichen, A. Madani, M. Abderrabba, P. Petkova, K. Boubaker, M. Amlouk, H. Bouchriha, Sensors and Actuators A, 227 (2015) 11.
- [61] W. Cao, R. Gerhardt, Solid State Ionics, 42 (1990) 213.
- [62] A. Godula, "proceeding of 2nd France-Deutschland fuel cell conference, Belfort (France), 29 Novembre-2December 2004.
- [63] V. M. Goldschmidt, V. 1958, Grochemistry, Oxford university press.
- [64] M.E. Lines and A. M. Glass, principles and applications of ferroelectrics and relates materials, 2001, Oxford university press.
- [65] P. Petkova, K. Boubaker, J. of Alloys and Compounds, 546 (5) (2013) 176-179.
- [66] Colantoni, L. Longo, K. Boubaker, D. Monarca, M. Cecchini, S. Cividino, A. Yumak, P. Biondi, S. Di Giacinto , G. Menghini, Mater. Res. Exp., 2 (2015) 035903.
- [67] Yumak, K. Boubaker, P. Petkova, U. Yahsi, J. of Molec. Struc., 1098 (2015) 255.
- [68] L. Ben Said, T. Larbi, A. Yumak, K. Boubaker, M. Amlouk, Materials Science in Semiconductor Processing, 40 (2015) 224.
- [69] D. Gherouel, S. Dabbous, K. Boubaker, M. Amlouk, Materials Science in Semiconductor Processing, 16 (2013) 1434.
- [70] M. Haj Lakhdar, B. Ouni, R. Boughalmi, T. Larbi, A. Boukhachem, A. Colantoni, K. Boubaker, M. Amlouk, Current Applied Physics, 14 (2014) 1078.
- [71] K. Boubaker, ISRN Nanomaterials, 2012, (2012) 4. Doi:10.5402/2012/173198.
- [72] K. Boubaker, Journal of Ceramics, 2013 (2013) 6.
- [73] K. Boubaker, M. Amlouk, Y. Louartassi, H. Labiadh, J. Aust. Ceram. Soc., 49 (2013)115.
- [74] K. Ben Messaoud, A. Gantassi, H. Essaidi, J. Ouerfelli, A. Colantoni, K. Boubaker, M. Amlouk, Adv. in Mater.Sci. and Engin. 2014 (2014) 1.
- [75] R. Mimouni, K. Boubaker, M. Amlouk, J. of Alloys and Compounds, 624 (2015) 189.
- [76] A. Bougrine, M. Addou, A. Kachouane, J.C. Bérnède, M. Morsli, Materials Chemistry and Physics, 91 (2005) 247.
- [77] C. M. Ghimbeu, M. Lumberras, M. Siadat, J. Schoonman, Materials Chemistry and Physics, 114 (2009) 933.
- [78] J. A. Jiménez, C. Zhao, Materials Chemistry and Physics, 147 (2014) 469.